Nanocavities in He implanted InP

M. Chicoine[a] and S. Roorda
Groupe de recherche en physique et technologie des couches minces (GCM), Département de physique, Université de Montréal C.P. 6128 succ. Centre-ville, Montréal, Québec, Canada H3C 3J7

R. A. Masut and P. Desjardins
Groupe de recherche en physique et technologie des couches minces (GCM), Département de génie physique, École polytechnique de Montréal C.P. 6079 succ. Centre-ville, Montréal, Québec, Canada H3C 3A7

(Received 19 May 2003; accepted 20 August 2003)

The formation of nanocavities in InP(001) by room-temperature He implantation and subsequent thermal annealing was studied using a combination of high-resolution x-ray diffraction (HRXRD) and cross-sectional transmission electron microscopy (XTEM) analyses. The nanocavities size and depth distributions were measured as a function of He ion dose ϕ_{He} (1×10^{16} to $9\times10^{16}\,cm^{-2}$) and ion energy E (25 to 70 keV), as well as annealing temperature T_a (600 to 750 °C) and time t_a (5 to 25 min). HRXRD scans from annealed samples indicate an expansion of the InP lattice, contrary to what is usually observed following heavy-ion implantation. The critical ϕ_{He} and T_a values for the formation of nanocavities were found by XTEM analysis to be between 1 and $2\times10^{16}\,cm^{-2}$ and between 600 and 620 °C, respectively. Cavities of diameter 4–50 nm with {110}, {101}, and {001} facets were obtained. Increasing T_a and t_a resulted in larger cavities and increasing ϕ_{He} produced a larger number of cavities. Furthermore we find that nanocavities are metastable as their size first increases with annealing temperature and time but then decreases until they disappear for $t_a > 25$ min at $T_a = 640$ °C or $t_a > 10$ min at $T_a = 750$ °C. Results are compared with similar work carried out on He-implanted silicon and differences between the two materials are explained in terms of defect diffusivity and surface energy, higher diffusivity enhancing cavity collapse and lower surface energy enhancing cavity growth. © *2003 American Institute of Physics.*
[DOI: 10.1063/1.1618354]

I. INTRODUCTION

Nanocavities can be formed in various ceramics and semiconductors by helium or hydrogen implantation followed by high temperature thermal annealing. Helium, which has a very low solubility in these materials segregates around defect sites created by ion implantation; upon high temperature annealing this situation leads to the formation of gas-filled cavities. Nanocavity growth is the result of the competition between the gas pressure inside the cavities and the surface tension of the gas-filled cavity. In the case of silicon, helium can diffuse out of the matrix and evaporate at the surface thus transforming helium-filled cavities into empty cavities. Various studies have shown this process to be strongly dependent upon the He dose.[1–3] The minimum He concentration required for cavity formation in silicon has been estimated to be $3.5\times10^{20}\,cm^{-3}$. At low concentrations ($<2\times10^{20}\,cm^{-3}$), small He-vacancy complexes are present after implantation but they may dissociate upon thermal annealing[4] so that most of the implanted He atoms diffuse out of the sample without contributing to cavity formation. This results in a low density of cavity clusters surrounded by strong strain fields.[3] Formation temperature T_a for low concentrations is around 700 °C. At higher concentrations ($>4\times10^{21}\,cm^{-3}$), small helium-filled cavities are already present during implantation. During subsequent thermal annealing He is released from the cavities and desorbs at the surface while the cavities coarsen.[5–7] At high doses (typically $\phi_{He}>1\times10^{17}\,cm^{-2}$, depending on parameters such as implantation energy, annealing temperature, etc.), the cavity number density becomes so high that the material above the implantation depth exfoliates.[8,9] He or H cavities have also been observed in several materials including GaP, InAs,[10] GaAs,[10,11] SiC,[12] MgO,[13] and InGaAs.[11] The general trends for cavities in these compounds are similar to what is observed in Si except for MgO, where the cavities are of rectangular shape while they are of faceted spherical shape in Si and III–V materials.

In this article, we present results on the formation of He cavities in InP(001) and compare them with results for Si(001). The cavities were created by He implantation followed by high-temperature thermal annealing and were studied by high-resolution x-ray diffraction (HRXRD) and transmission electron microscopy (TEM). It is found that cavity formation takes place at lower temperatures than in Si. The cavities exhibited {110}, {101}, and {001} facets. Their size increased with annealing temperature and time but they were metastable and disappeared after annealing for 25 min at 640 °C or 10 min at 750 °C. Material parameters that are relevant for cavity formation are He solubility and diffusivity, surface energy, and defect diffusivity in the matrix. Since helium is a small, closed-shell atom that interacts very weakly with other atoms, its solubility and diffusivity will only depend on the size of interstitial space and should be

[a]Electronic mail: martin.chicoine@umontreal.ca

 © 2003 American Institute of Physics

Downloaded 24 Oct 2003 to 132.204.64.75. Redistribution subject to AIP license or copyright, see http://ojps.aip.org/japo/japcr.jsp

similar in InP and Si. However defects and their diffusion are more complex in III–V materials in general. Defect creation by ion implantation and plastic deformation are also more efficient in InP than in Si.[14–16] We discuss the differences in cavity formation between InP and Si in terms of these properties.

II. EXPERIMENTAL DETAILS

InP(001) samples were implanted at room temperature with He ions of energies ranging from 25 to 70 keV and ion doses ϕ_{He} between 1×10^{16} and $9\times10^{16}\,cm^{-2}$. The focused helium beam was scanned over a 1.6×1.6 cm^2 area. The angle of incidence on the target was set to 7° to minimize channeling. The current density was about 1.5 $\mu A\,cm^{-2}$. The samples were annealed with T_a from 600 to 750 °C and t_a from 5 to 25 min in a metal-organic chemical vapor deposition (MOCVD) reactor under phosphorous overpressure with tertiarybutylphosphine (TBP) partial pressures ranging from 2.1×10^{-1} to 4.1×10^{-1} Torr. The chosen partial pressures of TBP are sufficient to inhibit surface degradation at all annealing temperatures used here.[17] Some samples were also treated by rapid thermal annealing (RTA) under Ar flow in an AG Associates Heatpulse 610 furnace, with the surface covered with a piece of InP.

The structural properties were investigated using HRXRD and TEM. HRXRD measurements were carried out using the Cu $K_{\alpha1}$ (λ=1.5406 Å) radiation from a Philips high-resolution five-crystal diffractometer with the monochromator aligned in its Ge (220) settings and a 0.45° receiving slit in front of the detector. TEM specimens were prepared in cross-section with ⟨110⟩ surface normals using mechanical polishing followed by room-temperature low-angle (4°) argon ion milling at 5 keV in a Gatan precision ion polishing system (PIPS). The ion energy was gradually reduced to 2.5 keV during the final stages of thinning to minimize radiation damage to the samples. Images were recorded at 300 kV on a Philips CM30 microscope using Fresnel contrast to observe the nanocavities.

III. RESULTS

A. TEM

As-implanted samples show no observable nanocavities and are characterized by a point defects band whose width and depth increase with ϕ_{He} and E, respectively. For an InP(001) sample implanted with $\phi_{He}=3\times10^{16}\,cm^{-2}$ at 40 keV, TEM micrographs exhibit a ≈165 nm wide band centered at a depth of 295 nm. For comparison, SRIM[18] simulations gives a calculated ion projected range (R_p) and longitudinal straggling of 300 and 130 nm, respectively, and maximum concentration of vacancies at 230 nm below the surface. Figure 1 shows a TEM image from the same sample annealed for $t_a=10$ min at $T_a=640$ °C under phosphorous overpressure. As seen on the micrograph, the near surface region shows considerable damage, containing a large number of dislocations and stacking faults (top defects). A 60 nm-wide band of nanocavities with diameters ranging from ≈8 to ≈18 nm is visible at a depth of 220 nm. The cavities are thus centered near the maximum concentration of vacancies predicted by SRIM, which has also been verified for implantations at $E=25$ and 70 keV for which R_p values are 210 and 445 nm, respectively. This is in agreement to what is observed in Si.[19] Finally, a ≈250 nm wide band of dislocation loops centered at a depth of 375 nm is observed. Selected area electron diffraction patterns taken in the different regions of the sample indicate that it is a single crystal.

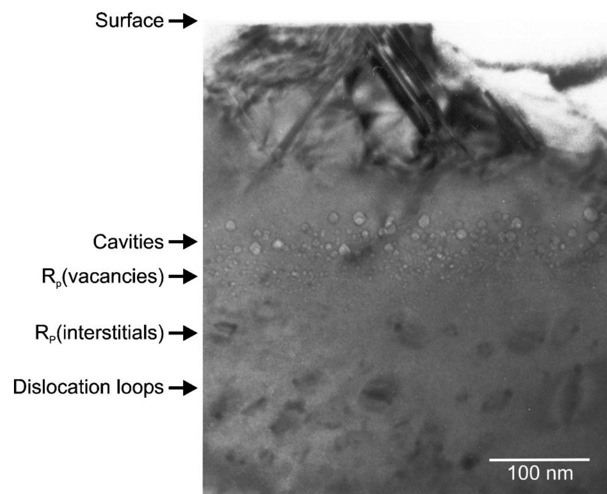

FIG. 1. TEM cross-section image with g near the $00\bar{2}$ orientation from an InP(001) sample implanted with $\phi_{He}=3\times10^{16}\,cm^{-2}$ at 40 keV and annealed 10 min at 640 °C.

Figure 2 shows a close-up of the cavity band from a sample implanted under the same conditions as in Fig. 1 but annealed at $T_a=620$ °C for $t_a=10$ min. In this case, the width of the cavity band is about 170 nm. The diameter of the cavities varies from ≈4 to ≈15 nm, except for one single cavity that is ≈28 nm in diameter. We found that the larger cavities are always located closer to the surface. That group of larger cavities will be chosen for the calculation of mean

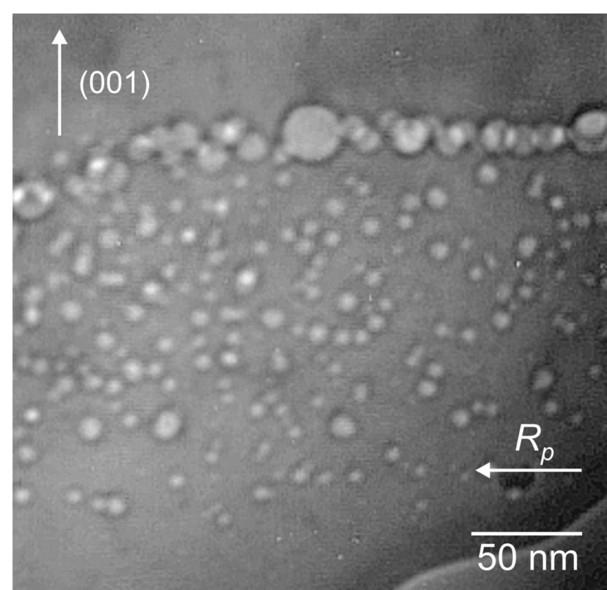

FIG. 2. Close-up of the cavity band of an InP(001) sample with g near the $00\bar{2}$ orientation implanted under the same conditions as in Fig. 1 and annealed 10 min at 620 °C. The arrow indicates the projected range R_p of the implanted ions.

Downloaded 24 Oct 2003 to 132.204.64.75. Redistribution subject to AIP license or copyright, see http://ojps.aip.org/japo/japcr.jsp

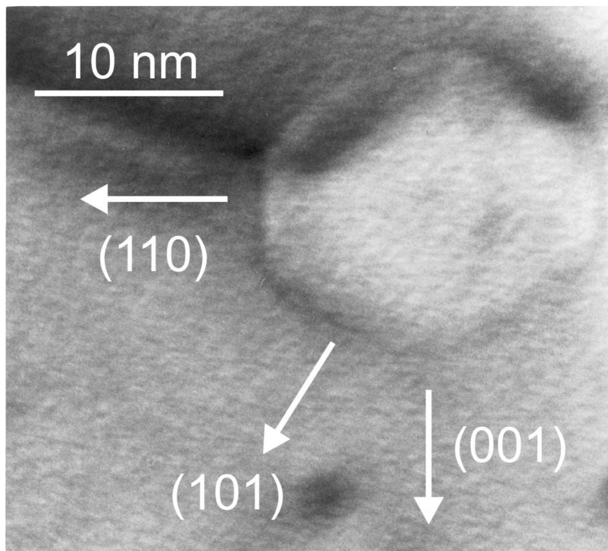

FIG. 3. Close-up of a cavity from the same sample as in Fig. 1 with g near the $00\bar{2}$ orientation.

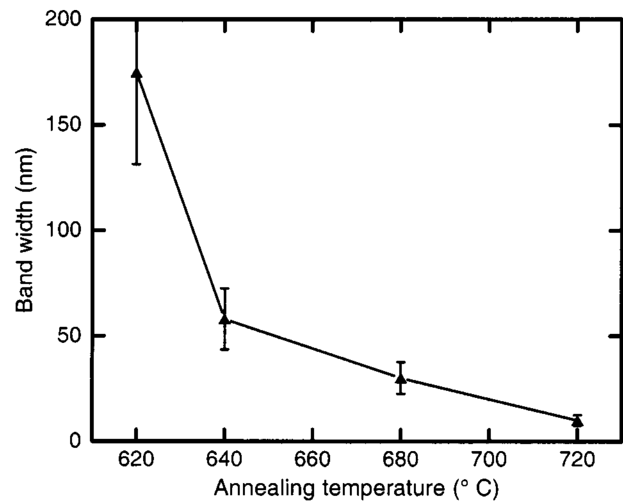

FIG. 5. Nanocavity band width as a function of annealing temperature for InP(001) implanted with $\phi_{He}=3\times10^{16}\,cm^{-2}$ at 25 keV and annealed for 10 min. The cavities centers are used for width calculation.

cavity diameter values in Figs. 4, 5 and 6 because, as it will be discussed in the next paragraph, those larger cavities grow with increasing T_a and t_a while the smaller ones shrink, so they are more representative of the growth process. Figure 3 shows a single cavity of ≈18 nm diameter terminated with {001}, {110}, and {101} facets, for the same annealing conditions as in Fig. 1.

Figure 4 presents the size of the largest cavities as a function of normalized annealing temperature and implantation energy for a constant dose of $3\times10^{16}\,cm^{-2}$ and after a 10 min anneal under TBP. Data for cavities in Si implanted with $\phi_{He}=1\times10^{17}\,cm^{-2}$ at 100 keV and vacuum annealed for 1 h are shown for comparison.[20,21] The temperature is normalized to the respective melting temperatures T_m (1333 K for InP and 1687 K for Si) to provide an approximate scaling for defect concentrations and diffusivities in these materials. The comparison is not perfect since for these conditions, cavities in Si have reached equilibrium at this temperature while this is not the case for InP but it nevertheless provides insights into the formation mechanisms in InP. No cavities were observed for InP samples annealed at $T_a=600\,°C$. The cavity diameter then increased with increasing T_a, from 620 to 720 °C until they abruptly disappeared at $T_a=750\,°C$, in contrast with data for Si. Figure 5 shows the cavity band width as a function of annealing temperature for samples implanted with $\phi_{He}=3\times10^{16}\,cm^{-2}$ at 25 keV. Comparing with Fig. 4, we see that the increase in cavity diameter is accompanied by a decrease of the cavity band width, the larger cavities always staying at approximately the same depth while growing and smaller cavities progressively disappearing, which could be explained by an Oswald ripening process.[22] At 720 °C, the band is just one cavity wide, of diameter ≈47 nm. Figure 6 shows the variation of the maximal cavity size as a function of t_a for fixed T_a (640 °C) and implantation conditions ($\phi_{He}=3\times10^{16}\,cm^{-2}$ at 40 keV). The diameter of the cavities increases from 11 nm at $t_a=5$ min to 23 nm after 15 min of annealing. However after 25 min, they had disappeared, leaving only dislocation loops in place of the cavities.

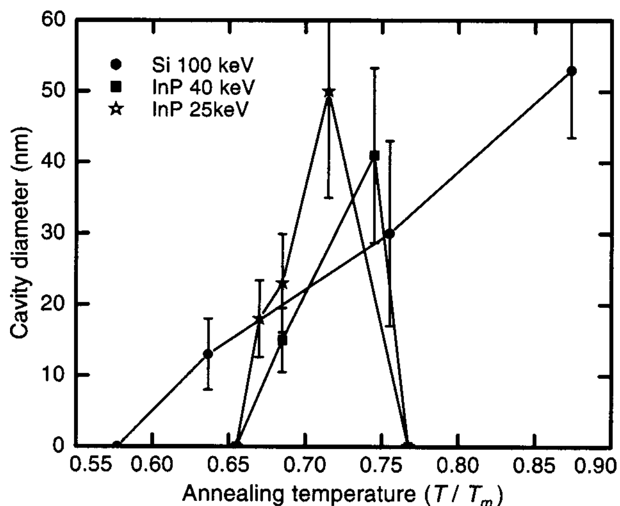

FIG. 4. Diameter of large cavities as a function of normalized annealing temperature for InP(001) implanted with $\phi_{He}=3\times10^{16}\,cm^{-2}$ at 40 keV (■) and 25 keV (★) and annealed for 10 min. Data for Si implanted with $\phi_{He}=1\times10^{17}\,cm^{-2}$ at 100 keV and annealed for 1 h (●) is shown for comparison (taken from Refs. 20 and 21). Error bars correspond to the standard deviation of cavities size.

Implantations with different ion doses were also investigated for samples annealed 10 min at 640 °C. No cavities were seen for samples implanted at $\phi_{He}=1\times10^{16}\,cm^{-2}$ whether it was at 25, 40, or 70 keV. Cavities were present for samples implanted at $2\times10^{16}\,cm^{-2}$ at 40 keV. For samples implanted at 40 keV and $\phi_{He}=9\times10^{16}\,cm^{-2}$, the mean depth of the cavities was the same as for the smaller doses but the cavity band was 300 nm wide, instead of 60 nm for $\phi_{He}=3\times10^{16}\,cm^{-2}$.

Finally, some samples were also annealed in a RTA furnace to compare the effect of temperature ramp-up, which were 120 °C/s in the RTA compared to about 2 °C/s in the MOCVD reactor. No significant differences in cavity size

Downloaded 24 Oct 2003 to 132.204.64.75. Redistribution subject to AIP license or copyright, see http://ojps.aip.org/japo/japcr.jsp

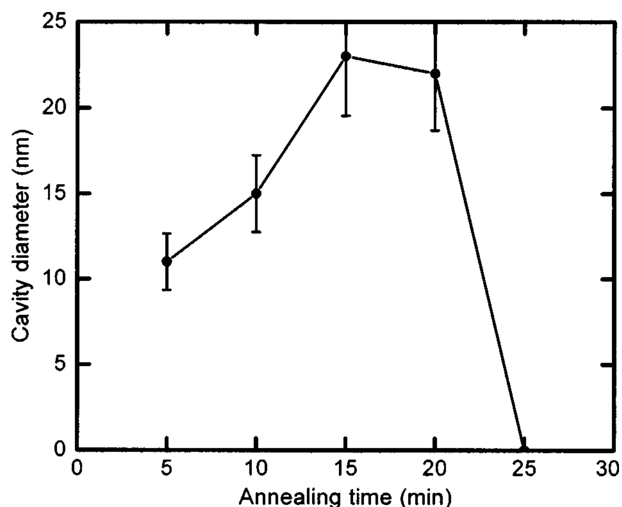

FIG. 6. Cavity diameter as a function of annealing time for InP(001) implanted with $\phi_{He}=3\times10^{16}\,cm^{-2}$ at 40 keV and annealed at 640 °C. Error bars correspond to the standard deviation of cavities size.

and distribution were observed between the two methods for samples annealed for 10 min at 620 °C, 5 min at 640 °C, 10 min at 640 °C, or 25 min at 640 °C. These results are in contrast with what was observed in Ref. 8 which described the exfoliation of He-implanted InP. In this article, the anneal temperature ramp-up rate had a large influence on the occurrence and degree of exfoliation. The difference could be due to the lower energies and doses used in our work.

B. HRXRD

Figure 7 shows 004 HRXRD rocking curves from InP(001) samples implanted with $\phi_{He}=3\times10^{16}\,cm^{-2}$ at 40 keV. The bottom curve (a) corresponds to an as-implanted sample. The narrow, high intensity peak at zero relative angle arises from the InP(001) substrate at depths beyond the

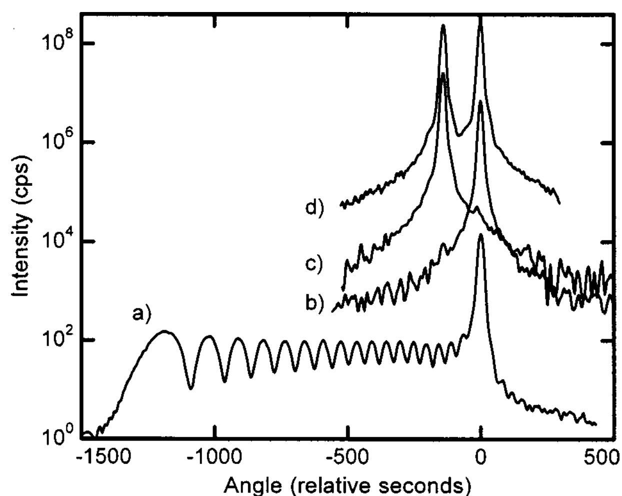

FIG. 7. HRXRD rocking curves from InP(001) samples implanted with $\phi_{He}=3\times10^{16}\,cm^{-2}$ at 40 keV (a) and annealed 15 min at 640 °C (b), (c), and (d). The curves from the annealed sample were taken on the nonimplanted part (b), only on the implanted part (c), and on the frontier between implanted and nonimplanted regions (d). They are vertically shifted for clarity.

ion projected range of 290 nm. The peak at the lowest angle stems from expanded material due to implantation damage and its shift from the substrate peak increases with ϕ_{He}. The peaks between the lowest angle peak and the substrate peaks are thickness fringes corresponding to the layer of material between the surface and the damaged zone. Their spacing increases from right to left because the strain in the damaged region increases progressively from the surface to the end of range of the implanted ions so that at low angles, the beam sees a smaller effective thickness. We note that the expansion observed here in InP corresponds to the usual behavior for implanted semiconductors but that it is different from the compaction that is usually observed for high energy heavy ion implantations in InP (see Ref. 14 for example). This difference in behavior could be related to the fact that for the *E* values used in this work, energy is lost mostly through direct collisions with target atoms while in the MeV-range energies, it is lost mostly through electronic excitations, which could result in different damage regimes in the crystalline substrate.[23]

Curves b–d in Fig. 7 correspond to 004 HRXRD patterns for an InP(001) sample that was implanted under the same conditions with the ion beam scanned only on half of its surface and annealed 15 min at 640 °C. The scans were taken with the x-ray beam directed only on the nonimplanted part (b), only on the implanted part (c), and on the frontier between implanted and nonimplanted regions (d). The full-width at half-maximum of the substrate peak in the nonimplanted region is 15.5 arc sec while it is 16.9 arc sec for the implanted part, indicating good crystalline quality for the implanted material.

A 145 arc sec shift of the InP peak to smaller angular values is observed for the implanted sample, as seen in curves (c) and (d). The presence of two distinct substrate peaks on these curves cannot be explained by lattice expansion in the implanted region because the fact that only one peak is seen in that region would imply that the signal coming from the substrate is less intense than the background level of the deformed InP layer peak. In order for this to be true, the thickness of the deformed region would have to be over 20 μm thick, according to x-ray diffraction simulations, which is very unlikely. Another possibility is that the sample is bent by 145 arc sec at the frontier between the implanted and nonimplanted regions. This bend could be caused by the volume expansion in the implanted region due to the space taken by nanocavities.

IV. DISCUSSION

A critical He implanted dose is necessary for cavity formation to take place.[1] In this work, this dose is found to be between 1×10^{16} and $2\times10^{16}\,He\,cm^{-2}$ for an ion energy between 25 and 70 keV and annealing temperatures above 620 °C. According to SRIM calculations, the maximum helium concentrations corresponding to the previous ion doses at 40 keV are 2.9×10^{20} and $5.8\times10^{20}\,cm^{-3}$, respectively. For comparison, the estimated critical dose for cavity formation in Si is $3.5\times10^{20}\,cm^{-3}$.[1,2] It was also observed that for a given ion energy and annealing conditions cavity bands

Downloaded 24 Oct 2003 to 132.204.64.75. Redistribution subject to AIP license or copyright, see http://ojps.aip.org/japo/japcr.jsp

were wider for higher ion doses. This is explained by the fact that a higher dose results in a wider region in which the He concentration is above a certain threshold concentration for cavity formation. In the further evolution of cavities with increasing annealing temperature and time, as described by Figs. 4, 5, and 6, the cavity diameter increases while the width of the cavity band decreases. Also, larger cavities grow at the expense of the smaller ones so that cavity growth could be driven by an Oswald ripening process.[22]

Cavity formation is more efficient in InP than in Si. From Fig. 4, it is seen that T_a/T_m values of 0.9 are required in order to obtain ≈50 nm-wide cavities in Si. Comparative T_a/T_m values for InP are ≈0.7. Overall, lower temperatures are necessary for He cavity formation in InP compared to Si. We propose that this is due to the lower surface energy of InP. For comparison, the measured surface energies of {110} planes in Si,[24] GaP, and GaAs (Ref. 25) are 1.43, 1.9, and 0.86 J/m^2, respectively, and InP surface energy is expected to be even lower because InP has less bonds per unit area and less energy per bond compared with GaAs and GaP. So, the necessary He pressure needed to sustain a cavity of a given dimension in Si should be at least twice the pressure needed in InP since pressure is proportional to surface energy for a given nanocavity radius. Therefore, cavity growth will be more efficient in InP than in Si.

A major difference between cavities in InP and Si is the dramatic collapse of cavities in InP when heated to a certain temperature for a sufficient time. We found no evidence in the literature for cavity collapse in other matcrials. We note for comparison purposes that cavities created under similar conditions in Si have been observed to be stable at temperatures as high as $T_a/T_m = 0.9$ for 5 h in Si.[21] In the case of InP(001), it is found that cavities have collapsed after an annealing time between 15 and 25 min at 640 °C. For comparable t_a and T_a for cavities in Si, helium has been completely evacuated from the cavities.[3] As has already been discussed in the introduction, He diffusivity should be similar in InP and Si so that the out-diffusion of He should also be the same in InP and Si. Therefore, it appears that cavities in InP shrink when He has out-diffused, which means that InP is not able to sustain empty cavities at high temperature. We propose that cavities in InP are filled by In and P atoms that diffuse in the material. Defects in InP are known to be highly mobile because of low cohesion energy.[15,26] The filling could also be enhanced by the In and P atoms already present as interstitials as irradiation damage due to He implantation. The measured defect interdiffusion rate for InP is $D_d \sim 10^{-11}\,\text{cm}^2/\text{s}$ at 725 °C (Ref. 26) while it is $D_d \approx 1.4 \times 10^{-15}\,\text{cm}^2/\text{s}$ for vacancies and $6.28 \times 10^{-15}\,\text{cm}^2/\text{s}$ for interstitials in Si at the same temperature.[27] This four orders of magnitude difference in defect mobility could explain why a similar cavity collapse has not been observed in Si. Cavity collapse could also be related to the high phosphorous partial vapor pressure of InP. At 750 °C, it is $\approx 3.6 \times 10^{-1}$ Torr.[17] For 50 nm nanocavities in equilibrium at 750 °C, this corresponds to about 1 P_2 molecule. Those P_2 molecules could interact with the surface of the nanocavities and enhance their filling.

V. CONCLUSION

In conclusion, we have created nanocavities in InP by helium implantation at doses $\phi_{\text{He}} > 2 \times 10^{16}\,\text{cm}^{-2}$ followed by thermal annealing at temperatures $T_a > 600\,°\text{C}$. Their size and distribution were studied as a function of ion energy, ion dose, annealing time, and annealing temperature. The cavities were metastable as they collapsed under annealing for 25 min at 640 °C or 10 min at 750 °C. The "processing window" for nanocavity formation in InP is thus limited; they are created for $T_a > 620\,°\text{C}$ but they collapse when T_a and t_a are large enough. It was also found that the InP lattice expands under $3 \times 10^{16}\,\text{cm}^{-2}$ He 40 keV implantation contrary to the compression which is usually observed for high-energy implantation.

Results were compared to data on cavity formation in Si found in the literature. The fact that the obtained cavities are larger in InP than in Si for similar He energy, ion doses, annealing temperatures, and times is attributed to the lower surface energy of InP. We also propose that the cavity collapse observed in InP and not in Si is due to the high defect diffusivity in InP, which facilitates In and P diffusion to fill the empty cavity after He out diffusion.

ACKNOWLEDGMENTS

The authors are grateful to Réal Gosselin and Pierre Bérichon for their technical assistance. This work benefited of grants from the NSERC of Canada and FCAR of Québec. P. Desjardins thanks the Canada Research Chair program for financial support.

[1] V. Raineri, P. G. Fallica, G. Percolla, A. Battaglia, M. Barbagallo, and S. U. Campisano, J. Appl. Phys. **78**, 3727 (1995).
[2] S. M. Myers and D. M. Follstaedt, J. Appl. Phys. **79**, 1337 (1996).
[3] P. F. P. Fichtner, J. R. Kaschny, R. A. Yankov, A. Mücklich, U. Kreissig, and W. Skorupa, Appl. Phys. Lett. **70**, 732 (1997).
[4] A. van Veen, H. Schut, R. A. Hakvoort, A. Fedorov, and K. T. Westerduin, Mater. Res. Soc. Symp. Proc. **373**, 499 (1995).
[5] C. C. Griffioen, J. H. Evans, P. C. de Jong, and A. van Veen, Nucl. Instrum. Methods Phys. Res. B **27**, 417 (1987).
[6] S. M. Myers, C. M. Foellstaedt, H. J. Stein, and W. R. Wampler, Phys. Rev. B **45**, 3914 (1992).
[7] V. Raineri, A. Battaglia, and E. Rimini, Nucl. Instrum. Methods Phys. Res. B **96**, 249 (1995).
[8] T. W. Simpson, I. V. Mitchell, G. O. Este, and F. R. Shepherd, Nucl. Instrum. Methods Phys. Res. B **148**, 381 (1999).
[9] M. Bruel, Nucl. Instrum. Methods Phys. Res. B **108**, 313 (1996).
[10] M. Chicoine, S. Roorda, and R. A. Masut, unpublished.
[11] D. M. Follstaedt, S. M. Myers, J. C. Barbour, G. A. Petersen, J. L. Reno, L. R. Dawson, and S. R. Lee, Nucl. Instrum. Methods Phys. Res. B **160**, 476 (2000).
[12] J. Chen, P. Jung, and H. Trinkaus, Phys. Rev. B **61**, 12923 (2000).
[13] B. J. Kooi, A. van Veen, J. T. M. D. Hosson, H. Schut, A. V. Fedorov, and F. Labohm, Appl. Phys. Lett. **76**, 1110 (2000).
[14] L. Cliche, S. Roorda, and R. A. Masut, Appl. Phys. Lett. **65**, 1754 (1994).
[15] L. Cliche, S. Roorda, G. E. Kajrys, and R. A. Masut, J. Appl. Phys. **79**, 2142 (1996).
[16] M. Chicoine, S. Roorda, L. Cliche, and R. A. Masut, Phys. Rev. B **79**, 2142 (1997).
[17] M. B. Panish and J. R. Arthur, J. Chem. Thermodyn. **2**, 299 (1970).
[18] J. F. Ziegler, J. P. Biersack, and U. Littmark, *The Stopping and Range of Ions in Solids* (Pergamon, New York, 1985).
[19] V. Raineri, S. Coffa, E. Szilágyi, J. Gyulai, and E. Rimini, Phys. Rev. B **61**, 937 (2000).
[20] F. Schiettekatte, C. Wintgens, and S. Roorda, Appl. Phys. Lett. **74**, 1857 (1999).

Downloaded 24 Oct 2003 to 132.204.64.75. Redistribution subject to AIP license or copyright, see http://ojps.aip.org/japo/japcr.jsp

[21] V. Raineri, M. Saggio, F. Frisina, and E. Rimini, Solid-State Electron. **42**, 2295 (1998).
[22] R. Delamare, E. Ntsoenzok, F. Labohm, A. van Veen, J. Grisolia, and A. Claverie, Nucl. Instrum. Methods Phys. Res. B **186**, 324 (2002).
[23] The energy lost by direct collisions and by electronic excitations can be calculated with SRIM (Ref. 18).
[24] D. J. Eaglesham, A. E. White, L. C. Feldman, N. Moriya, and D. C. Jacobson, Phys. Rev. Lett. **70**, 1643 (1993).
[25] C. Messmer and J. C. Bilello, J. Appl. Phys. **52**, 4623 (1981).
[26] J. E. Haysom, P. J. Poole, R. L. Williams, S. Raymond, and G. C. Aers, Solid State Commun. **116**, 187 (2000).
[27] T. Okino and T. Shimozaki, Physica B **273–274**, 509 (1999).

Downloaded 24 Oct 2003 to 132.204.64.75. Redistribution subject to AIP license or copyright, see http://ojps.aip.org/japo/japcr.jsp